GAVIN PUBLISHERS

Journal of Materials Science and Research

Liu Y, et al. J Mater Sci Res: JMSR-104.

Research Article

DOI: 10.29011/ JMSR-104. 100004

Molecular Dynamics Simulation of Temperature-Dependent Distribution of Gold Nano Particles on Ferroelectrics Substrate

Yue Liu[1*], Jiuyang Li[1], Jiahe Wang[2], Mohan Tang[2] Yuhong Qin[2], Yuejun Sun[1*]

[1]College of Materials Science and Engineering, Liaoning Technical University, Fuxin, China

[2]Lab of Mathematical Model, Beijing National Day School, Beijing, China

[*]**Corresponding authors:** Yue Liu, College of Materials Science and Engineering, Liaoning Technical University, Fuxin, China. Email: yueliu000@163.com

Yuejun Sun, Lab of Mathematical Model, Beijing National Day School, Beijing, China. Email: sunyuejun0001@163.com

Citation: Liu Y, Li J, Wang J, Tang M, Qin Y, et al. (2017) Molecular Dynamics Simulation of Temperature-Dependent Distribution of Gold Nano Particles on Ferroelectrics Substrate. J Mater Sci Res: JMSR-104. DOI: 10.29011/ JMSR-104. 100004

Received Date: 09 November, 2017; **Accepted Date:** 15 November, 2017; **Published Date:** 24 November, 2017

Abstract

Gold Nano Particles (GNPs) have been considered the widely used catalyst for chemical industry. However, the efficiency of the GNPs has been limited by the aggregation of the GNPs, as the active sites are only located on the surface of the catalyst particles. In this paper we report the surface aggregation dynamics of GNPs on ferroelectrics substrate. The ferroelectrics substrate and temperature could regulate the coverage of the GNPs. The method of reducing the particle size to obtain the dispersed morphology of GNPs was discussed by the dissipative particle dynamics method and density functional theory. The positive surface could offer more electrons on the GNPs and are responsible for the dispersed morphology of the GNPs.

Introduction

Gold Nano Particles (GNPs) are used as the photo catalyst and sensors for more than six decades [1]. GNPs own particular optical and catalytic properties especially compared with the bulk Au materials, since the active sites are only located on the surface of the catalyst particles [2-4]. Downsizing the GNPs to small clusters is awfully desirable to maximize their efficiency by utilizing gold particles up to the hilt [5-8]. The GNPs properties are strongly connected with the shape, size and morphology of the nano particles. The experimental results have already obtained the conclusion that the morphology of GNPs could be a key point to the catalyst properties. Varies experimental results about the morphology have been obtained, but the fabrication of GNPs was not easily controllable, the relationship between the fabrication detail and the morphology of GNPs have not been built sufficiently, especially in detail [9-12]. Controlled and large-scale synthesis of stable small clusters of GNPs remains a considerable challenge due to the metal atoms agglomerate at nano scale, resulting in a natural tendency for metal atoms to form larger clusters [13,14]. The temperature is one of the most important factor of fabrication, which will influence the morphology of Au particles visibly.

The fabrication of metal on the ferroelectric surface is also precursor to the development of devices that can harness the unique characteristics associated with polarizable materials, including both perovskite and related crystals [15-22]. Growth of nano-clusters and nano-crystals of noble metals has been observed at the surface of traditional ferroelectric such as strontium titanate ($SrTiO_3$) [23-25]. However, it is not clear where the nucleation of the metal atoms occurs. In this paper, the relationship between the fabrication temperature and morphology of Au particles on nontraditional perovskite crystals like $LiNbO_3$ have been discussed, the Au thin films coverage rate versus fabrication temperature has been researched. $LiNbO_3$ is currently widely used in a wide variety of existing device and its high surface charge density makes it attractive for use in other applications similar to those explored involving other metallic oxides and ferroelectrics. The growth dynamics of the Au thin films morphology on $LiNbO_3$ surface with opposite polarization have been uncovered by the Dissipative Particle Dynamics method, to illustrate the Au morphology dynamics at different temperatures.

Simulation method

In the Au thin film growth process among the experiment,

the relative positions and velocities of the particles in the $LiNbO_3$ substrate and Au thin films satisfy the proper conservation laws and symmetries, and the momentum transferred from the particles also satisfies the linear and angular conservations, which meet the demands of the DPD method.

In this work, the DPD method was applied to the solid molecular, which has agreed with the experiment results at our previous work [26]. As a result, we find the optimal deposition temperature and substrate orientation.

The Dissipative Particle Dynamics (DPD) method was optimized by Koelman and Hoogerbrugge, [27,28] which allows longer-time scale calculation and larger system simulation. Espanol R, and Warren P [29] The DPD method has been used in studying a surfactant among water molecular [30,31]. Ryjkina et al. [30] and Kuo et al. [31] reported that the DPD method can also be used in liquid molecular aggregation. The lithium niobate molecule and the gold atom were chosen to be the DPD particles to understand the gold nano particles morphology on the $LiNbO_3$ substrate. Assume that the lithium niobate molecules are in stoichiometry (Li-Nb-O_3) and electric neutrality under ideal target and oxygen atmosphere, and the total molecular number is 100 as a substrate.

The GNPs is set as 100-1000 particles in each simulation work. The particle numbers of GNP are related to the laser energy in the PLD system. The $LiNbO_3$ molecular lattice parameters are a = b = 0.515 nm, c = 1.3863 nm, and the average distance between the molecular is 1 nm in the substrate. In the two-dimensional simulation of a 10 nm×10 nm film. The simulation result is probably one shot of the laser pulse, which is important in the first growth stage of thin films [26]. Considering the ideal condition which does not include the defects and supposes that the particles at the boundaries are in balance. Approximately, the whole progress in PLD is designed to deposit on the $LiNbO_3$ surface of 100 nm_100 nm at different temperatures.

The unreconstructed $LiNbO_3$ (001) positive and negative surfaces are selected as the deposition surface. The final position of a DPD particle is determined by the force exerted on it. The time evolution of the process follows Newton's law. A DPD particle is affected by the neighbor DPD particles via three non-bonded forces: a conservative force F_{ij}^{C}, a dissipative force F_{ij}^{D}, and a random force F_{ij}^{R}. Therefore, the effective force F_i acting on particle *i* is given by [28].

$$F_i = \sum_{i \neq j} F_{ij}^{C} + \sum_{i \neq j} F_{ij}^{D} + \sum_{i \neq j} F_{ij}^{R} \qquad (1)$$

where *i, j* represents the DPD particles of the Au atom and lithium niobate molecule, respectively. The F_{ij}^{C} is a repulsive central force with a maximum value a_{ij} as shown in Ref [30].

$$F_{ij}^{C} = a_{ij}\left(1 - \frac{r_{ij}}{r_c}\right)e_{ij} \qquad (2)$$

where a_{ij}, e_{ij}, r_{ij}, r_c are the maximum repulsive parameter, the unit vector, the distance between particles *i* and *j,* and the cutoff radius, respectively.

To calculate F_{ij}^{C}, a_{ij} must be calculated. Here the interaction parameter is obtained by considering the mean pair contact interaction energy E^{ij}_{MIX}(T) between lithium niobate molecules and silicon atoms. First, the mixing energy $E^{ij}_{MIX}(T)$ was calculated between two DPD particles *i* and *j* according to [31]

$$E_{MIX}^{ij}(T) = \left[Z_{ij} \left\langle E_{ij}(T) \right\rangle + Z_{ji} \left\langle E_{ji}(T) \right\rangle - Z_{ii} \left\langle E_{ii}(T) \right\rangle - Z_{jj} \left\langle E_{jj}(T) \right\rangle \right] / 2 \qquad (3)$$

Where the Zs are the coordination number of each DPD particle pair. The averaged pair interaction energy <*E(T)*> was optimized. The electron state was set as the ground state, default spin and B3LYP based on the Density Function Theory (DFT) by using the Gaussian software. And the basis set is 6-31G and no charge, since detail information is a key factor to the accuracy, the electron spin was considered and the energy between particle *i* and *j* was optimized. These calculated averaged mixing energies are used to obtain the Flory-Huggins interactions parameter $\chi_{ij}(T)$ as shown in [32]

$$c_{ij}(T) = E^{ij}_{MIX}(T) / RT \quad (4)$$

And the χ parameter is used to determine the maximum repulsive force a_{ij} between particle *i* and *j* given as [32]

$$a_{ij}(T) = a_{ii} + 1.451 c_{ij} k_B T \quad (5)$$

Where the terms are offered by interaction between the pure DPD particles *i* (a_{ii}=15k_BT) [33], and end to this the calculation of $a_{ij}(T)$ can be defined. The force F^D_{ij} and F^R_{ij} are responsible for the conservation of total momentum in the system. To calculate F^D_{ij} and F^R_{ij}, the parameters are derived from Groot and Warren [33]. The whole programming is realized in Mathematica, and the detail was offered in our former work [26].

Results and discussion

It has been demonstrated that a strong interaction between the deposited metal and supported material plays a vital role in the stabilization of supported catalysts [34]. Despite the controllable deposition process during PLD experiment, atomic diffusion and agglomeration are still possible and probable, if a weak interaction exists between the atoms and the support, thus resulting in a large particle. It has been reported in the literature that doping the graphene lattice with N can enhance the Pt-C support interaction energy, resulting in highly stable Pt catalysts [35-37].

The comparison of energy between the positive and negative surface is presented in (Table 1), The energies were obtained through DFT method. The strongest interaction was at the distance of 1 nm; therefore, the electrons will form a strong bond. The electrons combination energy there is stronger on positive surface than negative. As the reference mentioned above, the positive surface will form smaller particles since the energy is stronger than the negative surface at all the distance. This verified that Au-positive surface bond is stronger and more difficult to break, and the positive surface will prevent the movement of Au by the high bond energy and increase the dispersion of the particles.

Positive		Negative	
Distance (nm)	**Energy(eV)**	**Distance (nm)**	**Energy (eV)**
0.5		0.5	1009.74852
1.0	979.942545	1.0	946.445557
1.5	921.236717	1.5	900.642205
2.0	882.565429	2.0	868.336042
2.5	855.312869	2.5	844.842028
3.0	835.148555	3.0	827.110048
3.5	819.651413	3.5	813.283610
4.0	807.377837	4.0	802.208625
4.5	797.419613	4.5	793.139851
5.0	789.178857	5.0	785.577389
5.5	782.246654	5.5	779.174262
6.0	776.334151	6.0	773.682377
6.5	771.231615	6.5	768.919729
7.0	766.783127	7.0	764.749799
7.5	762.870375	7.5	761.068181
8.0	759.401970	8.0	757.793666
8.5	756.306203	8.5	754.862129
9.0	753.526013	9.0	752.222263
9.5	751.015435	9.5	749.832521
10.0	748.737021	10.0	747.658903
20	726.1475172	20	725.8510816
30	718.2105163	30	718.0744224
40	714.1596913	40	714.081876
50	711.7019964	50	711.6517013
100	706.7238199	100	706.7109945
200	704.2026298	200	704.1993914
500	702.6794323	500	702.6789111
1000	702.1699339	1000	702.1698046

Table 1: The comparison of energy between the positive and negative surface is presented in table.

Applying the DPD method, the Au and LiNbO3 particles are modeled by the Gaussian software, in (Figure 1) The arrow indicates the polarization direction. This figure shows the interaction between the Au particles and the LiNbO3 polarized surface. In this result, the polarization is alternated with different orientation.

To verify the polarized surface effect on the Au dispersion, the DPD method is applied to uncover the surface morphology. The 2-D surface morphology of the Au nano particles are displayed in (Figure 2).

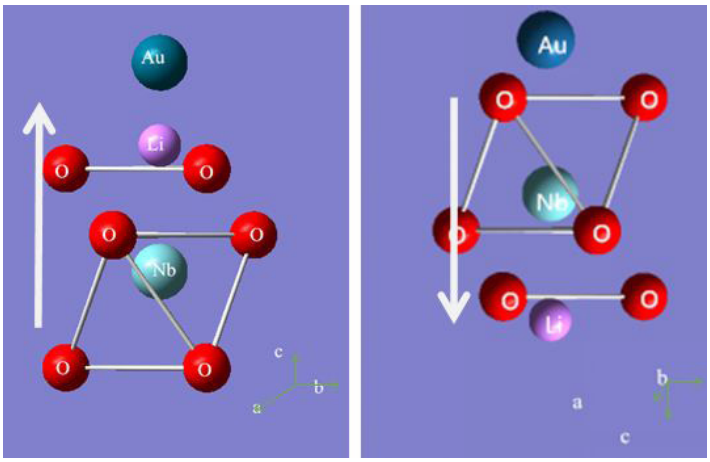

Figure 1: The molecular model of Au and LiNbO3 molecule with different polarization direction. The white arrow is the polarization direction.

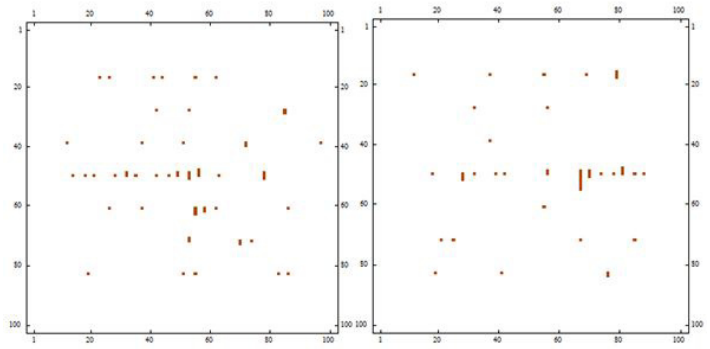

Figure 2: The GNP morphology on different polarized surface: 1) Positive surface and 2) negative surface. The unit is Å on each axis.

The positive surface offered more electrons on the GNPs since the Li atoms could carry more electrons which are not immobilized, and could form more bonds between the Li^+ deficiency vacancy and Au particles. With the strong connection, the GNPs formed smaller particles stably and reduced the aggregation of GNPs since the bond between the Au is weaker than the Au-Li deficiency vacancy on the positive surface than the negative.

We further calculated the coverage of GNPs on positive and negative surface under different temperature. The coverage is defined by the GNPs particle numbers divided by the $LiNbO_3$ molecular numbers.

As shown in (Figure 3a), when the deposition number is 100, the variation of the 500 K-1000 K coverage of Au on $LiNbO_3$ crystal, red dots represent the coverage of the positive surface of lithium niobate crystal; black dots represent the coverage of the negative surface of $LiNbO_3$ crystal. when the GNPs number is 100, with increasing temperature in the range of 550 K-1000 K, the coverage of positive surface is larger than the negative one; the coverage increases both linearly, thus we could obtain the change of GNPs by alternating the spontaneous polarization of ferroelectrics substrate.

In (Figure 3b), the dispersed GNPs particles increased to 1000, and the difference between the positive and negative surface coverage was more remarkable. The effect becomes obvious in the range of more GNPs, since the polarization and GNPs interact strongly. This is due to the increase of GNPs numbers, which offered more atoms to the substrate, and the interaction between the Li^+ deficiency vacancy and GNPs on the positive surface becomes even more violent.

It could be seen that the increase of temperature added the coverage linearly on both surface. This dynamic is related to the bond between the gold and $LiNbO_3$ molecular, the Li deficiency vacancy is much easier than O atoms to connect with the Au atoms, and the positive surface always occupied the most Li deficiency vacancy, as reported by YF Kong et al. [38]. The molecular dynamics simulation of Au on $LiNbO_3$ substrate explained the experiment results obtained by the Satyaveda et al. [1], and this will further help forecast the morphology of Au on different ferroelectrics substrate.

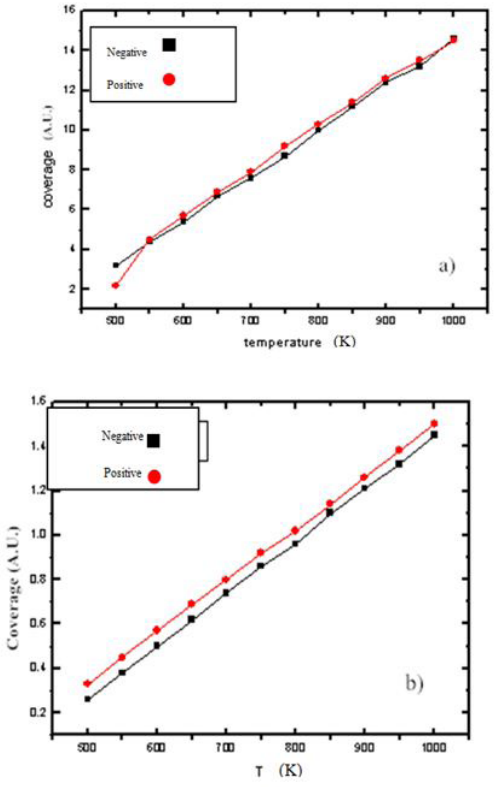

Figure 3(a-b): the coverage rate versus the temperature on polarized surface: a) the Au atoms are 100 and b) the Au atoms are 1000.

Conclusion

In summary, the positive surface of LiNbO3 offered more electrons to the bond between Li+ deficiency vacancy and GNPs, which makes more dispersed morphology than the negative surface, and which explained the experiment and first principle calculation results. And the alternation of polarization could change the coverage of GNPs at large temperature range. The coverage of GNPs could be adjusted by the temperature linearly.

References

1. Satyaveda Bharath C, Thomas Pearl P (2010) Growth of ultrathin layers of Au on $LiNbO_3$(0001) measured with atomic force microscopy. Surface Science 604: 713-717.
2. Cheng N, Stambula S, Da W, Banis M. Jian N, et al. (2016) Platinum single-atom and cluster catalysis of the hydrogen evolution reaction. Nature Communications: 1-9.
3. Pacchioni G, Giordano L, Baistrocchi M (2005) Charging of metal atoms on ultrathin MgO/Mo (100) films. Physical Review Letters 94: 6104.
4. Hansen KH, Worren T, Stempel S, Laegsgaard E, Baumer M, et al. (1999) Palladium Nanocrystals on Al_2O_3: Structure and Adhesion Energy. Physical Review Letters 83: 4120-4123.
5. Cooper VR, Kolpak AM, Yourdshahyan Y, Rappe AM (2005) Supported metal electronic structure: Implications for molecular adsorption. Physical Review B 72: 1-4.
6. Watanabe Y, Okano M, Masuda A (2001) Surface Conduction on Insulating $BaTiO_3$ Crystal Suggesting an Intrinsic Surface Electron Layer. Physical Review Letters 86: 332-335.
7. Hutter E, Fendler JH (2004) Exploitation of Localized Surface Plasmon Resonance. Advanced Materials 16: 1685-1706.
8. Afonso CN, Serna R, Ballesteros JM, Petford-Long AK, Doole DC (1998) Synthesis by pulsed laser deposition of metallic nanoclusters embedded in an amorphous host. Applied Surface Science 129: 339-343.
9. Gonzalo J, Perea A, Babonneau D, Afonso CN, Beer N, et al. (2005) Competing processes during the production of metal nano particles by pulsed laser deposition. Physical Review B 71: 1-8.
10. Warrender JM, Aziz MJ (2007) Kinetic energy effects on morphology evolution during pulsed laser deposition of metal-on-insulator films. Physical Review B 75: 794-802.
11. Donnelly T, Doggett B, Lunney JG (2006) Pulsed laser deposition of nano structured Ag films. Applied Surface Science 252: 4445-4448.
12. Silly F, Castell MR (2005) Selecting the shape of supported metal nanocrystals: Pd huts, hexagons, or pyramids on $SrTiO_3$(001). Physical Review Letters 94: 046103.
13. Mackus AJM, Verheijen MA, Leick N, Bol AA, Kessels WMM (2013) Influence of oxygen exposure on the nucleation of platinum atomic layer deposition: consequences for film growth, nanopatterning, and nanoparticle synthesis. Chemical Materials 25: 1905-1911.
14. Yang M, Li S, Wang Y, Herron JA, Xu Y, et al. (2014) Catalytically active Au-O(OH)x-species stabilized by alkali ions on zeolites and mesoporous oxides. Science 346: 1498-1501.
15. Garra J, Vohs JM, Bonnell DA (2009) The effect of ferroelectric polarization on the interaction of water and methanol with the surface of $LiNbO_3$ (0001). Surface Science 603: 1106-1114.
16. Garra J, Vohs JM, Bonnell DA (2009) Defect-mediated adsorption of methanol and carbon dioxide on $BaTiO_3$(001). J ournal of Vacuum Science & Technology A. 27: 13-17.
17. Habicht S, Nemanich RJ, Gruverman A (2008) Physical adsorption on ferroelectric surfaces: photoinduced and thermal effects. Nanotechnology 19: 495303.
18. Hanson JN, Rodriguez BJ, Nemanich RJ, Gruverman A (2006) Fabrication of metallic nanowires on a ferroelectric template via photochemical reaction. Nanotechnology 17: 4946-4949.
19. Yun Y, Pilet N, Schwarz UD, El Altman (2009) Comparison of the interaction of Pd with positively and negatively poled $LiNbO_3$(0001). Surface Science 603: 3145-3154.
20. Yun Y, Kampschulte L, Li M, Liao D, Altman EI (2007) Effect of Ferroelectric Poling on the Adsorption of 2-Propanol on $LiNbO_3$(0001). Journal of Physical Chemistry C 111: 13951-13956.
21. Yun Y, Altman EI (2007) Using ferroelectric poling to change adsorption on oxide surfaces. Journal of the American Chemical Society 129: 15684-15689.
22. Bharath SC, Pimputkar KR, Pronschinske AM, Pearl TP (2008) Liquid crystal deposition on poled, single crystalline lithium niobate. Applied Surface Science 254: 2048-2053.
23. Wang CM, Shutthanandan V, Zhang Y, Thomas LE, Baer DR (2004) Precipitation of Au nanoclusters in $SrTiO_3$ by ion implantation. Journal of Applied Physics 95: 5060-5068.
24. Silly F, Castell MR (2006) Bimodal Growth of Au on $SrTiO_3$ (001). Physical Review Letters 96: 086104.
25. Silly F, Castell MR (2005) Growth of Ag icosahedral nanocrystals on a $SrTiO_3$(001) support. Applied Physics Letters 87: 5840.
26. Yue L, Haonan Z, Zidong P, Yongfa K, Jingjun X (2015) Molecular dynamic simulations of surface morphology and pulsed laser deposition growth of lithium niobate thin films on silicon substrate. Chinese Physics B 24: 464-467.
27. Warrender JM, Aziz MJ (2003) X-Ray Characterization of Nanostructured Semiconductor Short-Period Superlattices. Material Research Society Symponium Process 749 w311.
28. Hoogerbrugge PJ, Koelman JM (1992) Simulating microscopic hydrodynamics phenomena with dissipative particle dynamics. Europhysics Letter 19: 155.
29. Espanol R, Warren P (1995) Statistical-mechanics of dissipative particle dynamics. Europhysical Letter 30: 191.
30. Koelman JM, Hoogerbrugge PJ (1993) Dynamic simulations of hard-sphere suspensions under steady shear. Europhysical Letter 21: 363.
31. Ryjkina E, Kuhn H, Rehage H, Felix M, Peggau J (2002) Molecular dynamic computer simulations of phase behavior of non-ionic surfactants. Angew Chem Int Ed 41: 983-986.
32. Kuo MY, Yang HC, Hua CY, Chen CL, Mao SZ, et al. (2004) Molecular dynamic computer simulations of phase behavior of non-ionic surfactants. Chem Phys Chem 41: 983-986.

33. Groot R, Warren P (1997) Dissipative particle dynamics: Bridging the gap between atomistic and mesoscopic simulation. Journal of Chemical Physical 107: 4423-4435.

34. Qiao B, Li JX, Wang A, Xu CQ, Tao JL, et al. (2015) Ultrastable single-atom gold catalysts with strong covalent metal-support interaction (CMSI). Nano Research 8: 2913-2924.

35. Kondo T, Suzuki T, Nakamura J (2011) Nitrogen doping of graphite for enhancement of durability of supported platinum clusters. Journal Physical Chemical Letter 2: 577-580.

36. Chen YG, Wang J, Liu H, Li R, Sun X, et al. (2009) Enhanced stability of Pt electrocatalysts by nitrogen doping in CNTs for PEM fuel cells. Electrochemical Communication 11: 2071-2076.

37. Bulushev DA, Zacharska M, Lisitsyn AS, Podyacheva OY, Fredrik S, et al. (2016) Single atoms of Pt-group metals stabilized by n-doped carbon nanofibers for efficient hydrogen production from formic acid. Acs Catalysis 6: 3442-3451.

38. Yongfa K, Jiachun D, Wanlin Z, Jinke W, Guangyin Z, et al. (1994) OH-absorption spectra in doped lithium niobate crystals, Physical Letter A 196: 128-132.